

A model for puffing/microexplosions in water/fuel emulsion droplets

Z. Nissar^a, O. Rybdylova^b, S.S. Sazhin^{b,*}, M. Heikal^{a,b}, A. Rashid B.A. Aziz^a, Mhadi A. Ismael^a

^a Center for Automotive Research and Electric Mobility, Universiti Teknologi PETRONAS, 32610 Seri Iskandar, Perak, Malaysia

^b Advanced Engineering Centre, School of Computing, Engineering and Mathematics, University of Brighton, Brighton, BN2 4GJ, UK

Abstract

A new analytical solution to the one-dimensional transient heat conduction equation in a composite spherically symmetric water-fuel emulsion droplet, suspended in a hot gas, is obtained. The Robin boundary condition at the surface of a droplet and conditions at the fuel-water interface are used. A water sub-droplet is assumed to be located at the centre of a fuel droplet, the radius of which was fixed at each time step; it could change at the next time step. The Abramzon and Sirignano model is applied for the approximation of the droplet evaporation process. This solution and the evaporation model are incorporated into a numerical code in which droplet heating/evaporation and the variable thermophysical properties are accounted for. The time instant at which the temperature at the fuel-water interface became equal to the boiling temperature of water is identified with the initiation of puffing, giving rise to microexplosion. This allowed us to compute the minimal microexplosion delay time. The new solution is applied to a typical case of puffing/microexplosion of water/diesel emulsion droplets in high temperature gas. It is shown that the new model allows us to understand better the underlying physics of the processes leading to puffing/microexplosion. The experimental observations of the microexplosion delay time for various initial droplet sizes are shown to be compatible with the predicted values of this time. It is shown that puffing/microexplosions are expected well before the droplet surface temperature reaches the boiling temperature of n-dodecane. The numerical code can be potentially implemented into Computational Fluid Dynamics codes, which can be applied to the modelling of other fuel and water/fuel blends.

Keywords: n-dodecane; droplet heating; heat conduction equation; microexplosion; puffing; diffusional entrapment; boiling

Nomenclature

A	function used in (A1.26)
B	function used in (A1.26)
$B_{T(M)}$	Spalding heat (mass) transfer number
c	specific heat capacity (J/ (kg K))
$F(t, \xi)$	$u(t, R)$ (K·m)
f_n	coefficients introduced in formula (4.5)
h	convective heat transfer coefficient (W/(m ² K))
$H(t)$	$\frac{h(t)}{k_f} - \frac{1}{R_d}$ (1/m)
h_0	$\frac{h \cdot R_d}{k_f} - 1$
$H_0(t)$	$\frac{h(t) \cdot R_d}{k_f} - 1$
k	thermal conductivity (W/ (m K)) or weighting factor
L	latent heat of evaporation (J/kg)
M	molar mass (g/mol)
Nu	Nusselt number
P	thermal radiation term in (3.1) (K/s)
p	ambient pressure (atm or Pa)
$\tilde{P}(\xi)$	$P(R)$ (K/s)
p_n	coefficients used in (4.7) (K·m ³ /s)
q_n	coefficients introduced in Formula (4.6) (K·m)
R	distance (m)
$R_{w(d)}$	radius of the water (fuel) droplet (m or μm)
Re	Reynolds number
t	time (s)
T	temperature (K)
$u(t, R)$	$T(t, R) \cdot R$ (K·m)
$V(t, \xi)$	function introduced in Formula (A1.14) (K·m)

$V_{fr,w}$	volume fraction of water
v_n	eigenfunctions defined in (4.2)
$\ v_n\ ^2$	norm of v_n (W/ (m·K))
X	mole fraction
Y	mass fraction

Greek Symbols

κ	thermal diffusivity (m ² /s)
Δt	time step (s)
β_n	function introduced in Formula (4.10)
$\theta_n(t)$	function defined by Equation (4.3) (K·m)
λ_n	eigenvalues found from (4.9)
$\mu(t)$	$\frac{R_d}{k_f} (h(t) \cdot T_g + \rho_t \cdot L_f \cdot \dot{R}_d)$ (K)
$\mu_0(t)$	$R_d \cdot \mu(t)$ (K·m)
ζ	R/R_d
ρ	density (kg/m ³)

Subscripts

avg	average
b	boiling
d	droplet
eff	effective
f	fuel
g	ambient gas
hom	homogeneous
l	liquid
p	constant pressure
ref	reference conditions
s	surface
w	water
0	initial conditions

1 Introduction

Water/diesel emulsions have gained much attention as their application allows the simultaneous reduction of NO_x and soot. The addition of water reduces the adiabatic flame temperature, which inhibits the formation of NO_x [1, 2]. As water evaporates, it supplies hydroxy (OH) radicals to the combustion process, thereby increasing the oxidation rate and reducing soot formation [1, 2]. The application of these emulsions increases brake thermal efficiency by 6% and reduces NO_x and particulate emissions by 30%. Also, their application allows for a reduction of unburnt hydrocarbons by 70% [3, 4]. The degree of atomization and the penetration of the fuel spray plays a vital role in enhancing the overall combustion efficiency [5]. Atomization is known to increase the interfacial area of a fuel jet [6]. This directly affects the heat/mass transfer rates between droplet and ambient gas [6], which govern the efficiency of the combustion process. After the penetration of primary and secondary droplets inside a combustor, the degree of atomization can be further enhanced with the help of microexplosions [1, 2, 6].

Microexplosion is a phenomenon observed in water-diesel emulsion droplets and is caused by the diffusional resistance of the liquid fuel leading to entrapment of the dispersed component (water) inside the diesel droplet interior [6]. The droplet temperature is limited by the critical temperatures of leading diesel fuel components, which are much higher than the boiling temperature of water [6-8]. The embedded water droplets are distributed unevenly within the parent droplet and tend to accumulate near the droplet core. As the pressure inside the bubble, formed at the surface of the boiling water sub-droplet, increases, it grows causing thinning of the droplet surface; eventually the vapour bubble punches through the surface of the diesel droplet, resulting in destruction of the surface of the parent droplet [9]. If the phenomenon leads to total disintegration of fuel droplets, it is called microexplosion, and if it is localised in a specific region of the droplet, it is known as puffing [10].

The idea of microexplosions in water-fuel emulsions dates back to 1965 [2]. Ivanov and Nefedov observed that the evaporation of a fuel droplet accelerates on the addition of water. Law et al. [6, 7] investigated microexplosions in burning water-in-diesel emulsion droplets with diameters of about 1 mm to develop an efficient hybrid fuel for internal combustion engines which can have better anti-knock performance. During the experiments, it was found that the internal nucleation was enhanced during the unstable droplet generation mode, which was accompanied by ligament absorption in the aft region of the droplet [8, 11]. The role of microexplosions and their effects on the combustion and vaporisation behaviour of isolated multicomponent droplets have been widely discussed in the literature [7, 8, 12-15]. It was found that parameters such as ambient pressure, ambient temperature and the concentration of volatile components influence microexplosions. For water-in-diesel emulsion droplets, it was observed that microexplosions become more likely with increasing ambient pressure [12, 16]. This could be related to the fact that at higher pressures droplets can reach higher temperatures due to an elevation in the boiling points of diesel components at the surface without causing any significant change in the superheat limit of water entrapped within it. Microexplosions occurred for a specific range of ambient temperatures [8]; it was noted that at higher ambient temperatures the rate of droplet vaporisation is too high for microexplosions to occur, while at low temperatures, superheating does not occur. Microexplosion did not occur if the concentration of the volatile components, which determine the energy available for microexplosion, was too large or too small [17]. If the concentration of the volatile components is too large, the droplet evaporates and does not reach high surface temperatures. The probability of microexplosion increased when the radii of water sub-droplets increased and did not occur at all in the case of microemulsions as they tend to behave more like solutions [12, 18-21]. When the droplets traverse a spray environment under the influence of turbulent eddies, Sheng et al. [17] found that a single microexplosion initiates the simultaneous microexplosion of neighbouring droplets. This leads to the uniform initiation of microexplosions throughout the combustor. It was argued that microexplosions could be the dominant mode of secondary breakup in water-in-diesel fuel sprays, which can be used in combustors [1, 6, 10, 22]. However, there is a dearth of experimental data to support this.

Law [6] suggested that the distribution of temperature and species within the droplets should be estimated to assess the likelihood of occurrence of microexplosions. The modelling of microexplosions involves droplet heating, bubble nucleation, bubble growth, and droplet breakup. Although models developed in [23-25] are instrumental in understanding the physical background of microexplosion/puffing, their usefulness for engineering applications is less obvious. Moreover, in spray combustion calculations, where millions of such droplets undergo heating and puffing/microexplosions, it would be technically impossible to use such models due to the need for substantial computational resources. A number of authors, including [26, 27], suggested simplified models of the phenomenon. The model suggested in [27] is applicable to the analysis of the final stage of the phenomenon when water in fuel

droplets has evaporated. In this case, the problem focuses on the effect of the expanding water vapour on the liquid fuel shell surrounding it. The analysis of the stability of the system was performed under the assumption that the shell is spherical at the beginning of the process. This made it possible for the author of [27] to estimate the numbers and average diameters of the droplets, produced as a result of the instability development. This number depended on the initial thickness of the shell. The rather restrictive assumptions used when developing this model make it rather difficult to validate (see [15] for further discussion of this matter).

In contrast to the above-mentioned models, the focus of the model developed in [28] is on the prediction of the time to puffing/microexplosion; the parameter that is particularly important for practical engineering applications. In this model it is assumed that a small water sub-droplet is placed in the centre of a fuel droplet, and both droplets are spherically symmetric. The surface temperature of the fuel droplet is fixed, and fuel evaporation is not accounted for. The transient heat transfer equation is solved inside the droplet, using the Dirichlet boundary condition at its surface. The time when the water surface temperature reaches the boiling temperature of water is identified with the beginning of the puffing/microexplosion process. The predictions of the model were shown to be consistent with observations of relatively small composite droplets (with diameters less than about 1 mm), but not with those of larger droplets [15, 28]. The main restriction of this model, and of the model suggested in [27], lies in the assumption that a water sub-droplet is located exactly in the centre of the fuel droplet, which is not supported by the direct observation of composite droplets in the general case [15].

Apart from this restriction, the model developed in [28] has several other important limitations. Two of these limitations appear to be particularly important. Firstly, the fuel droplet surface temperature was fixed, which is not consistent with most observations [29]. Secondly, the problem was solved using the Dirichlet boundary conditions, while Robin boundary conditions are known to describe more accurately the heating of droplets. The aim of this paper is to describe a new model for puffing/microexplosion, using the same assumptions as the model developed in [28], but free from the above-mentioned two limitations.

The basic ideas behind the new model are presented in Section 2. Key equations and approximations are summarised in Section 3. The new analytical solution to the transient heat conduction equation in the liquid phase is presented in Section 4. The computer algorithm using this solution is described in Section 5. Applications of the new algorithm are discussed in Section 6. In Section 7, we summarise the most important results of the paper.

2 Description of the new model

As in the model described in [28], in our new model it is assumed that both fuel droplet and water sub-droplet are spherically symmetric, as schematically shown in Fig. 1. Although we appreciate the limitation of this approximation

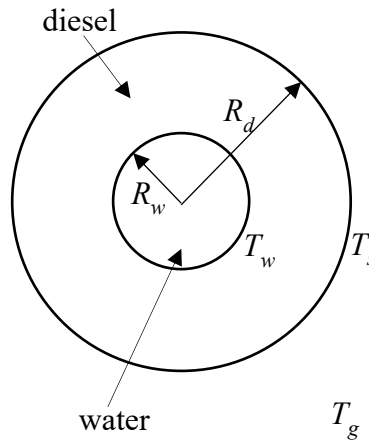


Fig. 1 Schematic of a water/diesel emulsion droplet in a gas, where R_w is the radius of the water sub-droplet inside the fuel droplet of radius R_d . T_w and T_s are the temperatures at the surface of the water sub-droplet and at the surface of the fuel droplet, respectively. T_g is the ambient temperature.

(see the discussion in the previous section) we cannot abandon it. R_d is constant during individual time steps; but it can change at the following time steps due to droplet evaporation, in the general case. The effects of swelling are ignored in our analysis. T_w and T_s are the temperatures at the water-fuel interface and at the surface of the fuel droplet respectively. At the droplet surface, $T_s=T(t,R_d)$ depends on time [29]. The effect of the surface regression due to evaporation at individual time steps is not accounted for (see [30, 31] for the details). The thermophysical properties of diesel fuel are approximated by the properties of n-dodecane. Our analysis is restricted to stationary droplets.

The initiation of puffing is usually associated with the nucleation temperature the likelihood of which is sensitive to the local temperature, and is expected to be achieved at the water-fuel interface [32-34]. At nucleation temperature, bubble nucleation rate can change from a negligible to a substantial value [28]. Researchers have argued that it is challenging to attain genuine homogeneous nucleation, which is the upper-limit of heterogeneous nucleation under gravity, as processes are complicated by buoyancy [35-37]. Due to the dearth of data, the time instant at which the temperature at the water-fuel interface attains the boiling temperature of water is identified with the initiation of puffing/microexplosions. It is also referred to as time to puffing or microexplosion delay time [28].

3 Key equations and approximations

Ignoring the effects of interaction between droplets and assuming that the temperature distribution inside the water-fuel domain is spherically symmetric and the domain is piecewise due to water-fuel interface R_w , the variation in temperature in this domain can be inferred from the solution to the transient heat conduction equation [28, 38, 39].

$$\frac{\partial T}{\partial t} = \kappa \left(\frac{\partial^2 T}{\partial R^2} + \frac{2}{R} \frac{\partial T}{\partial R} \right) + P(t, R), \quad (3.1)$$

where

$$\kappa = \begin{cases} \kappa_w = \frac{k_w}{c_w \cdot \rho_w} & \text{when } R \leq R_w \\ \kappa_f = \frac{k_f}{c_f \cdot \rho_f} & \text{when } R_w < R \leq R_d. \end{cases} \quad (3.2)$$

$P(t,R)$ is the thermal radiation term that takes into account the thermal radiation absorption (the droplet is assumed to be semi-transparent). This term will be ignored during analysis as the contribution of this absorption to droplet heating was found to be less than 1% for temperatures less than or about 1000 K [40].

Equation (3.1) needs to be solved for $T \equiv T(t,R)$, using the initial/boundary conditions:

$$T|_{t=0} = \begin{cases} T_{w0}(R) & \text{when } R \leq R_w \\ T_{f0}(R) & \text{when } R_w < R \leq R_d, \end{cases} \quad (3.3)$$

$T(t,R)$ is twice continuously differentiable for $0 < t \leq t_L$ and $0 < R \leq R_d$; t_L is the droplet lifetime.

At the interface $R=R_w$, the following boundary conditions are used:

$$T|_{R=R_w^-} = T|_{R=R_w^+} \quad ; \quad k_w \frac{\partial T}{\partial R} \Big|_{R=R_w^-} = k_f \frac{\partial T}{\partial R} \Big|_{R=R_w^+} \quad (3.4)$$

At the interface $R=R_d$, the following boundary condition should be satisfied:

$$\left(k_f \frac{\partial T}{\partial R} + h \cdot T \right) \Big|_{R=R_d^-} = h \cdot T_g + \rho_{lf} \cdot L_f \cdot \dot{R}_d, \quad (3.5)$$

where L_f is the heat of evaporation and h is the convective heat transfer coefficient, describing heat reaching the surface of the droplet (assumed to be constant during individual time steps). Ignoring the effect of the Stefan flow it is estimated as [29]:

$$h = \frac{\bar{k}_g}{R_d}.$$

Assuming a unitary Lewis number, Equation (3.5) is supplemented by the following expression for the droplet evaporation rate [40, 41]:

$$\dot{m} = -4\pi R_d \frac{\bar{k}_g}{\bar{c}_{pg}} \ln(1 + B_M), \quad (3.6)$$

where B_M is the Spalding mass transfer number given as

$$B_M = \frac{Y_{fs} - Y_{f\infty}}{1 - Y_{fs}}, \quad (3.7)$$

the mass fraction of vapour fuel $Y_{f\infty}$ at a large distance from the droplet surface is ignored ($Y_{f\infty} = 0$). Approximation (3.6) and the assumption that $Nu=2$ were used to enable the comparison of our results with those obtained in [30, 43] where the same approximations were used.

Using Equation (3.6), the surface regression rate, \dot{R}_d , can be written in the form

$$\dot{R}_d = -\frac{\bar{k}_g \ln(1 + B_M)}{\rho_{fl} \cdot \bar{c}_{pg} \cdot R_d}. \quad (3.8)$$

To be consistent with (3.3) and (3.4), we write

$$T_{w0}(R_w) = T_{f0}(R_w). \quad (3.9)$$

The thermophysical properties of the liquid phase components as well as gas phase components are assumed to be constant during individual small time steps [40].

4 Analytical solutions

As mentioned earlier, in [28] the solution to Equation (3.1) was obtained assuming that T_s and R_d are constant throughout the whole process (the effect of evaporation was not taken into account) and using the Dirichlet boundary condition. In what follows, the model is generalised to consider the changes in T_s during individual time steps and R_d between time steps taking into account Equations (3.5) and (3.6). The solution to (3.1), using the initial/boundary conditions specified in Section 3, is presented as (see Appendix A):

$$T(\xi, t) = \frac{1}{R_d \cdot \xi} \sum_{n=1}^{\infty} \left(\theta_n(t) \cdot v_n(\xi) + \frac{\mu_0(t)}{1 + h_0} \xi \right), \quad (4.1)$$

where

$$v_n(R) = \begin{cases} \frac{\sin(\lambda_n \cdot \xi)}{\sin(\lambda_n \cdot \xi_w)} & \text{when } 0 \leq \xi \leq \xi_w \\ \frac{\sin(\lambda_n \cdot \xi + \beta_n)}{\sin(\lambda_n \cdot \xi_w + \beta_n)} & \text{when } \xi_w < \xi \leq 1, \end{cases} \quad (4.2)$$

$$\xi = \frac{R}{R_d} \quad ; \quad \xi_w = \frac{R_w}{R_d},$$

$$\theta_n(t) = (q_n + \mu_0(0) \cdot f_n) \exp\left(-\frac{\kappa \cdot \lambda_n^2 \cdot t}{R_d^2}\right) + \int_0^t \left(\frac{p_n}{R_d^2} + f_n \cdot \mu'_0(\tau)\right) \exp\left(\frac{\kappa \cdot \lambda_n^2 \cdot (\tau - t)}{R_d^2}\right) d\tau, \quad (4.3)$$

$$\mu_0(t) = \frac{R_d^2}{k_f} (h(t) \cdot T_g + \rho_l \cdot L_f \cdot \dot{R}_d) = \frac{R_d \cdot \bar{k}_g}{k_f} \left(T_g - L_f \frac{\ln(1 + B_M)}{\bar{c}_{pg}}\right), \quad (4.4)$$

$$f_n = \frac{1}{\|v_n\|^2} \left(\int_0^{\xi_w} \left(\frac{-\xi}{1+h_0}\right) \frac{\sin(\lambda_n \cdot \xi)}{\sin(\lambda_n \cdot \xi_w)} k_w d\xi + \int_{\xi_w}^1 \left(\frac{-\xi}{1+h_0}\right) \frac{\sin(\lambda_n \cdot \xi + \beta_n)}{\sin(\lambda_n \cdot \xi_w + \beta_n)} k_f d\xi \right), \quad (4.5)$$

$$q_n = \frac{1}{\|v_n\|^2} \left(\int_0^{\xi_w} R_d \cdot \xi \cdot T_0(\xi) \frac{\sin(\lambda_n \cdot \xi)}{\sin(\lambda_n \cdot \xi_w)} k_w d\xi + \int_{\xi_w}^1 R_d \cdot \xi \cdot T_0(\xi) \frac{\sin(\lambda_n \cdot \xi + \beta_n)}{\sin(\lambda_n \cdot \xi_w + \beta_n)} k_f d\xi \right), \quad (4.6)$$

$$p_n = \frac{1}{\|v_n\|^2} \left(\int_0^{\xi_w} R_d^3 \cdot \xi \cdot \bar{P}(\xi) \frac{\sin(\lambda_n \cdot \xi)}{\sin(\lambda_n \cdot \xi_w)} k_w d\xi + \int_{\xi_w}^1 R_d^3 \cdot \xi \cdot \bar{P}(\xi) \frac{\sin(\lambda_n \cdot \xi + \beta_n)}{\sin(\lambda_n \cdot \xi_w + \beta_n)} k_f d\xi \right), \quad (4.7)$$

$$\|v_n\|^2 = \frac{k_w}{2} \left(\xi_w \csc(\xi_w \cdot \lambda_n)^2 - \frac{\cot(\xi_w \cdot \lambda_n)}{\lambda_n} \right) + \frac{k_f}{4} \csc(\beta_n + \xi_w \cdot \lambda_n)^2 \left(2 - 2\xi_w + \frac{-\sin(2(\beta_n + \lambda_n)) + \sin(2(\beta_n + \xi_w \cdot \lambda_n))}{\lambda_n} \right). \quad (4.8)$$

Positive eigenvalues λ_n are found from the solution to the following equation:

$$\lambda \cos(\lambda + \beta) + h_0 \sin(\lambda + \beta) = 0, \quad (4.9)$$

where

$$\beta_n = \cot^{-1} \left(\frac{(k_f - k_w)}{k_f \cdot \xi_w \cdot \lambda_n} + \frac{k_w \cot(\xi_w \cdot \lambda_n)}{k_f} \right) - \xi_w \cdot \lambda_n, \quad (4.10)$$

$n=1, 2, 3 \dots, 0 < \lambda_1 < \lambda_2 \dots$

$$h_0 = \frac{h \cdot R_d}{k_f} - 1 = \text{constant} > -1, \quad h(t) = \frac{\bar{k}_g \cdot Nu}{2R_d}. \quad (4.11)$$

When the properties of water are assumed to be identical to those of fuel (homogeneous droplets), Solution (4.1) reduces to the one presented previously in [30, 42] (see Appendix B).

5 Algorithm

The solution algorithm, which we used, is summarised below.

- (1) Assume that the values of p and T_g are known. The value of R_w is assumed to be constant throughout the droplet lifetime; water swelling is ignored.
- (2) Compute the values of $T_{avg(w)}$ and $T_{avg(f)}$ using volume averaging given by the relation

$$T_{avg(w)} = \int_0^{\xi_w} \frac{3\xi^2 \cdot T(\xi)}{\xi_w^3} d\xi, \quad (5.1)$$

$$T_{avg(f)} = \int_{\xi_w}^1 \frac{3\xi^2 \cdot T(\xi)}{1 - \xi_w^3} d\xi. \quad (5.2)$$

- (3) Calculate the thermophysical properties of water and liquid fuel using $T_{avg(w)}$ and $T_{avg(f)}$ from the initial distribution of temperatures in the liquid phase or using values inferred from the previous iteration; these include c_{pfl} , c_{pwl} , ρ_{fl} , ρ_{wl} , k_{fl} , k_{wl} and $L_f(T_s)$. The approximations for the transport properties of the components are the same as in [40, 42].
- (4) Use the Clausius-Clapeyron equation to find the mole and mass fractions of the gas phase components (n-dodecane and air) using the equations:

$$X_i = \frac{1}{p} \exp \left[\frac{L_i}{R_u} \left(\frac{1}{T_{b,i}} - \frac{1}{T_s} \right) \right] \quad (5.3)$$

$$Y_i = \frac{X_i \cdot M_i}{\sum_j X_j \cdot M_j}, \quad (5.4)$$

where p is ambient pressure (in atm) and $R_u = 8.3145 \text{ J} \cdot \text{mol}^{-1} \cdot \text{K}^{-1}$.

- (5) Compute the values of the reference temperature T_{ref} and reference composition Y_{ref} in the gas phase using the standard '1/3 rule'.

$$T_{ref} = T_s + \frac{(T_\infty - T_s)}{3}; \quad Y_{ref} = Y_s + \frac{(Y_\infty - Y_s)}{3}, \quad (5.5)$$

where subscripts s , ∞ refer to the values at the surface of the droplet and ambient gas, respectively. For n-dodecane vapour, Y_∞ is assumed to be zero.

- (6) Calculate \dot{m} .
- (7) Compute the Nusselt number for the gas phase and h_0 using (4.11). It is assumed that $\text{Nu} = \text{constant} = 2$.
- (8) Find λ_n and β_n using (4.9) and (4.10); use Equation (4.1) to find the temperature distribution inside the droplet after time step Δt .
- (9) Replace $T_s = T(1)$, $T_0(\xi) = T(\xi)$ and $R_d = R_{d,old} + \dot{R}_d \cdot \Delta t$ for the next iteration; where $R_{d,old}$ is the droplet radius at the beginning of Δt .
- (10) Return to step 2; repeat for the next Δt . Continue until $T(\xi_w) = 373.15 \text{ K}$.

The number of recursions multiplied by Δt will give us the value of the puffing/microexplosion delay time.

6 Analysis

The analysis was performed for a stationary water-in-diesel emulsion (WIDE) droplet assuming a unitary Lewis number in the gas film without accounting for thermal radiation. The thermophysical properties of n-dodecane were used to approximate those of diesel fuel.

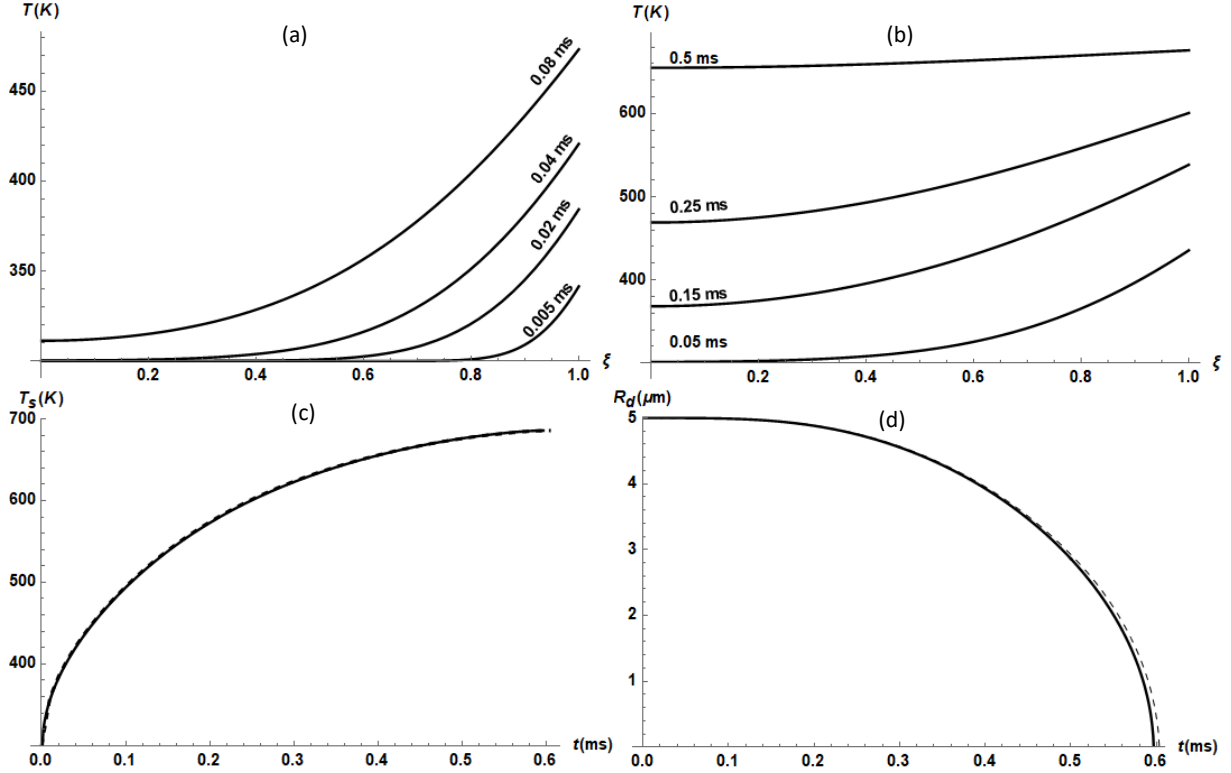


Fig. 2 Plots showing the comparison between the results predicted by the new model and the model presented in [30]. The results are presented for n-dodecane droplets heated and evaporated in air ($M_a = 29$ kg/kmole. $M_f = 170$ kg/kmole ($C_{12}H_{26}$)) for $R_{d0} = 5$ μm , $T_0 = 300$ K, $T_g = 1000$ K, $p = 3000$ kPa; (a) and (b) represent the temperature distribution $T(\xi)$ at different time instants, (c) and (d) show the variation of T_s and R_d (μm) with time (ms). The predictions of the current model are shown as solid curves, those of the model described in [30] as dashed curves'

Firstly, we verified the predictions of our code by considering a spherical domain (droplet) filled entirely with liquid n-dodecane. The computations were carried out on one 3.3 GHz Kernel using Wolfram Mathematica v 12.0 . The series in Equation (4.1) converged well for 90 terms for all the cases. The number of terms needed for the convergence of $T(\xi)$ depends on the time step Δt which was taken as 1 μs . The ambient temperature and ambient pressure were taken as 1000 K and 3000 kPa, respectively. Over 1000 time steps were used. The initial radius of the droplet was $R_{d0} = 5$ μm and the initial droplet temperature was taken equal to 300 K. The results of our calculations are shown in Fig. 2(a)-(d). The temperature distributions shown in Fig. 2(a) and (b) are in excellent agreement with Fig. 8, reported in [31], and Fig. 3(b) in [30], respectively. The results shown in Fig. 2(c, d) are also consistent with Fig 4 (a, b) reported in [30]. The predicted maximum surface temperature, 685.8 K, is the same as found in [30, 43]. Note that, in Fig. 2(d) the offset between the curves is the result of a different step size for Δt .

For analysis of a composite droplet of diesel and water, the droplet initial temperature and ambient gas temperature were taken as 300 K and 700 K, respectively. The ambient pressure was set to 101.325 kPa and the volume fraction of water $V_{f,w}$ was taken as 15%, as in the experiments described in [28]. It is assumed that puffing/microexplosion will occur when the fuel-water interface temperature becomes equal to the boiling point of water, i.e. when $T(\xi_w) = T_{bw}$. ξ is R normalised by the initial droplet radius R_{d0} .

Fig. 3 (a) shows the spatiotemporal temperature distribution at several time instants using the new model. Note the sharp change in the slopes of the curves at ξ_w (fuel-water interface). It can be observed that as the droplet heats up, ξ_w shifts and tends to merge with the droplet surface. $\xi_{w(i)}$ and $\xi_{w(f)}$ represent the interface between n-dodecane and water at the initial and later stages, respectively. The changes in this parameter are attributed to shrinking of droplets

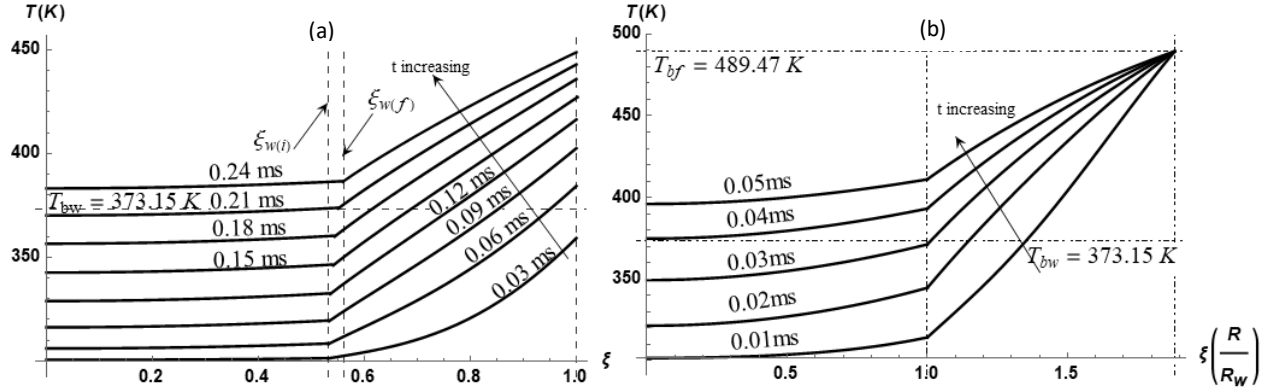


Fig. 3 Plots of $T(\xi)$ at several time instants for $R_{d0} = 5 \mu\text{m}$, $T_0 = 300 \text{ K}$, $T_g = 700 \text{ K}$, $p = 1 \text{ atm} = 101.325 \text{ kPa}$, $V_{fr,w} = 15\%$; (a) refers to the results obtained using the new model (b) shows the results obtained using the model described in [25]. Note different normalisations in (a) and (b).

due to evaporation. The microexplosion delay time for this particular case is 0.21 ms. The results presented in Fig. 3 (b) were obtained using the model developed in [28] in which the Dirichlet boundary conditions were assumed at the surface of the droplet and the effects due to changes in the droplet surface temperature and evaporation were ignored. The microexplosion delay time for this case is 0.036 ms. The parameters of the model were the same as for the case mentioned earlier ($R_{d0} = 5 \mu\text{m}$, $T_0 = 300 \text{ K}$, $T_g = 700 \text{ K}$, $p = 1 \text{ atm} = 101.325 \text{ kPa}$, $V_{fr,w} = 15\%$).

A comparison of Fig. 3 (a) and Fig. 3 (b) shows that the microexplosion delay time inferred from calculations using the new model is about 6 times greater than that inferred from calculations using the old model. This difference is attributed to the fact that the temperature at the surface of the droplet used in the analysis of [28] was much higher than that inferred from calculations using the new model. In [28], it was assumed that the temperature at the droplet surface is fixed (it does not depend on time). It can be seen that in Fig. 3 (a) the slope of the curves in the region ξ_w to 1 changes from concave upwards to concave downwards as heating progresses. This can be linked to the changes in heat fluxes shown in Fig. 4. The values of heat flux were obtained by calculating the derivatives of temperature, as in the approach used in [44]. In this figure, the heat fluxes entering at ξ_w and 1 at various times are shown. The shift in concavity occurs because heat flux entering at ξ_w increases and exceeds heat flux values at 1. At ξ_w , heat flux increases until $t \approx 0.145 \text{ ms}$, and then starts to decrease.

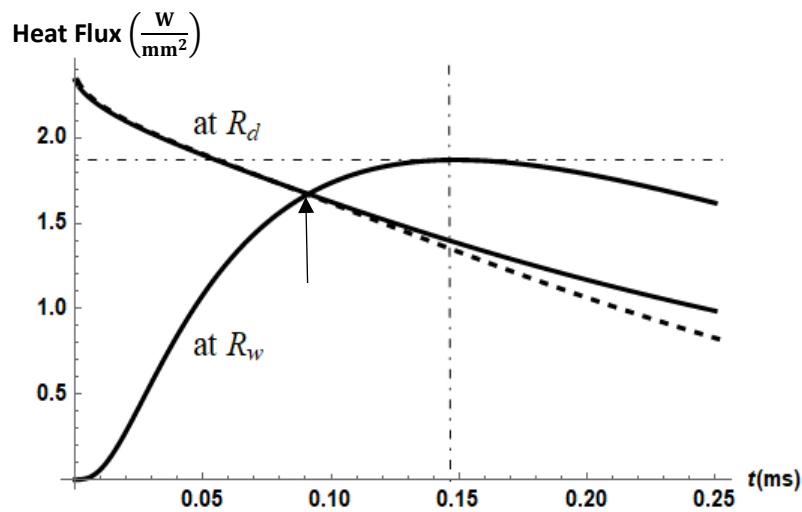


Fig. 4 Heat flux (W/mm^2) vs time (ms), inferred from calculations using the new model, for a composite droplet (solid) and pure n-dodecane droplet (dashed).

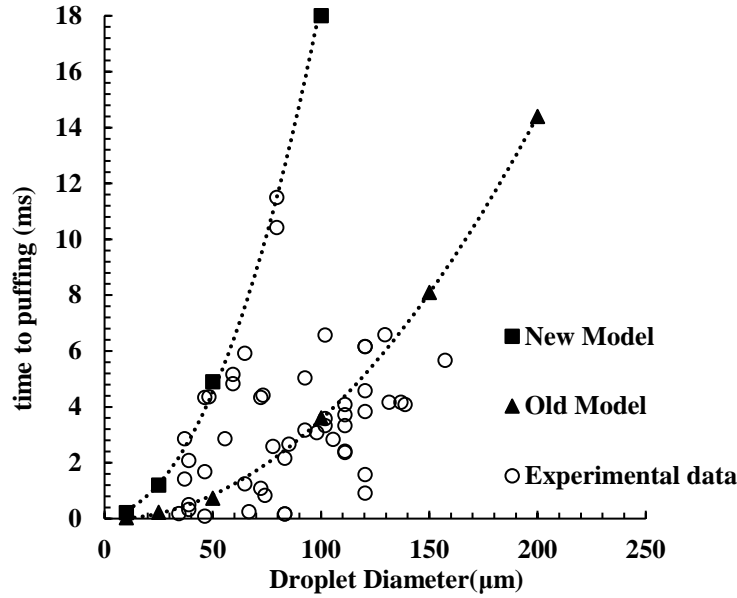


Fig. 5 A comparison between the times to puffing (ms) inferred from calculations using the new and previous models as the functions of the droplet diameters (μm) and the experimentally observed values. Calculations were performed using the same parameters as in Fig. 3

Calculations similar to those that produced the results shown in Fig. 3 were performed for droplets of various diameters using both new and previous models. The results are presented in Fig. 5. The same experimental conditions as in [22, 28] ($T_0 = 300$ K, $T_g = 700$ K, $p = 1$ atm = 101.325 kPa, $V_{fr,w} = 15\%$) were used. As can be seen in Fig. 5, the models predict rather different times to puffing/microexplosion, although both models predict an increase in this time as the droplet diameter increases. The new approach predicts longer times than the previous model which can be attributed to lower temperatures at the droplet surface inferred from the calculations using the new model. It can be seen that the points referring to experimental observations lie between the results inferred from the calculations using the new model and those using the model suggested in [28]. Note that both old and new models only describe correctly the trends in the experimental data, and not the values of individual times to puffing/microexplosion. This is something that we expected, remembering the very stringent assumptions which were made when developing these models.

The apparent overprediction of the time to puffing by the new model can be attributed to the important assumption made in the model that the water sub-droplet is located exactly at the centre of the n-dodecane droplet (see the relevant discussion in Section 1). In realistic cases, the water sub-droplet is likely to be shifted relative to the centre of the fuel

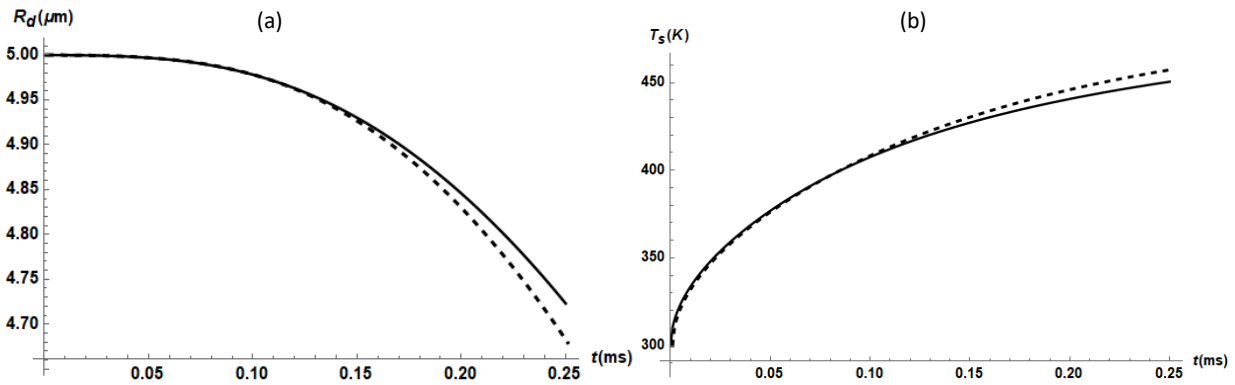


Fig. 6 (a) R_d (μm) vs time (ms); (b) T_s (K) versus time (ms), using the same conditions as in Fig. 3; composite droplet (solid), pure n-dodecane droplet (dashed).

droplet (cf. the results of observations of microexplosions described in [15, 45]), which would lead to a substantial reduction in the time to puffing. All the experimental observations are found to be below those predicted by the new model. As can be seen, no experimental values overshoot the values predicted by the new model. The effect of composite droplets on their heating/evaporation is demonstrated in Fig. 6. All parameters were taken to be the same as in the previous case ($T_0=300$ K, $T_g=700$ K, $p=1$ atm=101.325 kPa, $V_{fr,w} = 15\%$). Fig. 6 (a) presents the evolution of droplet radius with time. It can be seen that the droplet evaporation rate increases gradually with time thereby causing a reduction in droplet radius. It is found that the droplet radius reduces by about 3.2% before puffing/microexplosion is expected. The rate of droplet evaporation increases at the later stage of the process mainly due to higher values of surface temperature T_s , as presented in Fig. 6 (b). As can be seen from this figure, puffing/microexplosion takes place well before the surface attains the boiling point of n-dodecane. The surface temperature when puffing/microexplosion is expected was found to be 441.071K which is much lower than the n-dodecane boiling temperature used in the model suggested in [25]. The comparison of the curves for composite droplets and pure droplets, Fig. 6 (b), shows that the surface temperature changes slightly faster in the latter case.

7 Conclusion

A novel model for puffing/microexplosion of emulsion droplets is suggested. In this model, it is assumed that a water sub-droplet is entrapped in the centre of a fuel droplet, and the analytical solution to the one-dimensional transient heat conduction equation, which describes heat transfer from the surface of the droplet into the liquid phase, is used at each time step. This solution uses the Robin boundary condition at the droplet surface and the conditions at the water-fuel interface. Surface regression due to evaporation at the droplet surface is accounted for, but the effects of swelling of water and fuel are ignored. It is assumed that the time to puffing/microexplosion is equal to the time required to heat the water-fuel interface to the boiling point of water.

The code was verified using the model for homogeneous droplet heating and evaporation developed earlier. The predictions of the new model for the emulsion droplets were compared with those of the previously developed model which was based on the Dirichlet boundary condition at the droplet surface and in which the effects of changes in the droplet surface temperature and evaporation were ignored. The new model predicts longer times to puffing/microexplosion than those predicted by the previously developed model. The experimental observations of the microexplosion delay times for various initial droplet diameters were found to be below the predicted values. This is attributed to the expectation that water sub-droplets are not precisely positioned at the fuel droplet centre, which would lead to a large reduction in the time to puffing/microexplosion. A significant reduction in the droplet radius, due to evaporation, was noted before predicted puffing/microexplosion. It was observed that microexplosion/puffing takes place well before the surface attains the boiling point of n-dodecane. The suggested numerical algorithm can be used for the development of computational fluid dynamics (CFD) codes.

Conflict of interests

None

Acknowledgements

This work is a result of collaboration between the University of Brighton (supported by the EPSRC, UK, Grants EP/M002608/1 and EP/R012024/1), and the Centre for Automotive Research and Electric Mobility (CAREM) of the Universiti Teknologi PETRONAS (UTP) (supported by the ministry of higher education Fundamental Research Grant Scheme (FRGS) (Grant FRGS/1/2017/TK10/UTP/01/2) and UTP Graduate Assistant (GA) studentship). The authors are grateful to Dr Tali Bar-Kohany for useful discussion of the paper and drawing their attention to the inaccuracies in some formulae.

Appendix A

Derivation of Equation (4.1)

Introducing the variable

$$u = T \cdot R \quad (\text{A1.1})$$

we can simplify Eq. (3.1) and initial/boundary conditions (3.3), (3.4) and (3.5) to:

$$\frac{\partial u}{\partial t} = \kappa \left(\frac{\partial^2 u}{\partial R^2} \right) + R \cdot P(R) \quad (\text{A1.2})$$

for $t \in [t_0, t_0 + \Delta t]$ and $R \in [0, R_d]$,

where

$$\kappa = \begin{cases} \kappa_w = \frac{k_w}{c_w \cdot \rho_w} & \text{when } R \leq R_w \\ \kappa_f = \frac{k_f}{c_f \cdot \rho_f} & \text{when } R_w < R \leq R_d \end{cases} \quad (\text{A1.3})$$

$$u|_{t=0} = \begin{cases} R \cdot T_{w0}(R) & \text{when } 0 \leq R \leq R_w \\ R \cdot T_{f0}(R) & \text{when } R_w < R \leq R_d, \end{cases} \quad (\text{A1.4})$$

$$u|_{R=R_w^-} = u|_{R=R_w^+} \quad ; \quad k_w(R_w \cdot u'_R - u)|_{R=R_w^-} = k_f(R_w \cdot u'_R - u)|_{R=R_w^+} \quad (\text{A1.4})$$

$$(u'_R + H(t) \cdot u)|_{R=R_d^-} = \mu(t), \quad (\text{A1.5})$$

$$H(t) = \frac{h(t)}{k_f} - \frac{1}{R_d} \quad \text{and} \quad \mu(t) = \frac{R_d}{k_f} (h(t) \cdot T_g + \rho_l \cdot L_f \cdot \dot{R}_d).$$

At the next stage, we introduce variable $\zeta = R/R_d$ and function $F(t, \zeta) = u(t, R)$ (this approach was used in [30] to reduce the problem with a moving boundary to one with a stationary boundary).

For $0 \leq R \leq R_d$; $0 \leq \zeta \leq 1$,

Using ζ and $F(t, \zeta)$ Equation (A1.2) can be rewritten as

$$R_d^2 \cdot F'_t = \kappa \cdot F''_{\zeta\zeta} + \xi \cdot \dot{R}_d(t) \cdot R_d \cdot F'_\xi + R_d^3 \cdot \xi \cdot \tilde{P}(\xi) \quad (\text{A1.6})$$

for $t \in [t_0, t_0 + \Delta t]$ and $\zeta \in [0, 1]$.

Ignoring the effect of evaporation during the individual time step (the term proportional to $\dot{R}_d(t)$ in Equation (A1.6)) but not in the boundary conditions, the expression (A1.6) can be rewritten as

$$R_d^2 \cdot F'_t = \kappa \cdot F''_{\zeta\zeta} + R_d^3 \cdot \xi \cdot \tilde{P}(\xi). \quad (\text{A1.7})$$

The initial/boundary conditions are presented as

$$F|_{t=0} = \begin{cases} R_d \cdot \xi \cdot T_{w0}(\xi) & \text{when } 0 \leq \xi \leq \xi_w \\ R_d \cdot \xi \cdot T_{f0}(\xi) & \text{when } \xi_w < \xi \leq 1, \end{cases} \quad (\text{A1.8})$$

where

$$\xi_w = \frac{R_w}{R_d},$$

$$F|_{\xi_w^-} = F|_{\xi_w^+} \quad ; \quad k_w(\xi_w \cdot F'_\xi - F)|_{\xi_w^-} = k_f(\xi_w \cdot F'_\xi - F)|_{\xi_w^+}, \quad (\text{A1.9})$$

$$(F'_\xi + H_0(t) \cdot F)|_{\xi=1^-} = \mu_0(t), \quad (\text{A1.10})$$

$$H_0(t) = H(t) \cdot R_d = \frac{h(t) \cdot R_d}{k_f} - 1 = h_0 = \text{constant} > -1, \quad (\text{A1.11})$$

$$\mu_0(t) = \mu(t) \cdot R_d = \frac{R_d^2}{k_f} (h(t) \cdot T_g + \rho_l \cdot L_f \cdot \dot{R}_d), \quad (\text{A1.12})$$

$$h(t) = \frac{\bar{k}_g \cdot Nu}{2R_d}. \quad (\text{A1.13})$$

$h(t)$ and h_0 are considered constant during the individual time step. For stationary droplets, ignoring the effects of evaporation on convective heating of droplets (assuming that the heat transfer Spalding number is small), we have $Nu=2$.

To convert the inhomogeneous boundary condition (Equation (A1.10)) into homogeneous ones, we introduce function $V(t, \xi)$ via the equation

$$F(t, \xi) = V(t, \xi) + \frac{\mu_0(t)}{1 + h_0} \xi. \quad (\text{A1.14})$$

Using (A1.14), we can rewrite (A1.7) as

$$R_d^2 \cdot V'_t = \kappa \cdot V''_{\xi\xi} - \frac{\dot{\mu}_0(t) \cdot R_d^2}{1 + h_0} \xi + R_d^3 \cdot \xi \cdot \bar{P}(\xi). \quad (\text{A1.15})$$

The initial/boundary conditions are presented as:

$$V|_{t=0} = R_d \cdot \xi \cdot T_0(\xi \cdot R_d) - \frac{\mu_0(t)}{1 + h_0} \xi, \quad (\text{A1.16})$$

$$T_0(\xi \cdot R_d) = \begin{cases} T_{w0}(\xi \cdot R_d) & \text{when } 0 \leq \xi \leq \xi_w \\ T_{f0}(\xi \cdot R_d) & \text{when } \xi_w < \xi \leq 1, \end{cases}$$

$$V|_{\xi_w^-} = V|_{\xi_w^+} \quad ; \quad k_w(\xi_w \cdot V'_\xi - V)|_{\xi_w^-} = k_f(\xi_w \cdot V'_\xi - V)|_{\xi_w^+}, \quad (\text{A1.17})$$

$$(V'_\xi + h_0 V)|_{\xi=1^-} = 0. \quad (\text{A1.18})$$

We look for the solution to (A1.15) in the form

$$V(t, \xi) = \sum_{n=1}^{\infty} \theta_n(t) \cdot v_n(\xi), \quad (\text{A1.19})$$

where eigenfunctions $v_n(\xi)$ form the full set of non-trivial solutions to the equation:

$$\frac{d^2 v}{d\xi^2} + \lambda^2 \cdot v = 0. \quad (\text{A1.20})$$

(A1.20) is to be solved using the following boundary conditions

$$v|_{\xi=0} = (v'_\xi + h_0 \cdot v)|_{\xi=1^-} = 0, \quad (\text{A1.21})$$

$$v|_{\xi_w^-} = v|_{\xi_w^+} \quad ; \quad k_w(\xi_w \cdot v'_\xi - v)|_{\xi_w^-} = k_f(\xi_w \cdot v'_\xi - v)|_{\xi_w^+} \quad (\text{A1.22})$$

The general solution to (A1.20) subject to these boundary conditions can be presented as:

$$v_n(\xi) = \begin{cases} A_1 \cos(\lambda \cdot \xi) + B_1 \sin(\lambda \cdot \xi) & \text{when } 0 \leq \xi \leq \xi_w \\ A_2 \cos(\lambda \cdot \xi) + B_2 \sin(\lambda \cdot \xi) & \text{when } \xi_w < \xi \leq 1. \end{cases} \quad (\text{A1.23})$$

Note that:

$$A_2 \cos(\lambda \cdot \xi) + B_2 \sin(\lambda \cdot \xi) = \sqrt{A_2^2 + B_2^2} \sin\left(\lambda \cdot \xi + \tan^{-1}\left(\frac{A_2}{B_2}\right)\right). \quad (\text{A1.24})$$

From (A1.21) we have $A_1 = 0$. Making the following replacements $B_1 \rightarrow B$; $\sqrt{A_2^2 + B_2^2} \rightarrow A$ and $\tan^{-1}\left(\frac{A_2}{B_2}\right) \rightarrow \beta$, (A1.23) can be written as

$$v_n(R) = \begin{cases} B \sin(\lambda \cdot \xi) & \text{when } 0 \leq \xi \leq \xi_w \\ A \sin(\lambda \cdot \xi + \beta) & \text{when } \xi_w < \xi \leq 1. \end{cases} \quad (\text{A1.25})$$

From the first equation in (A1.22) we have

$$B \sin(\lambda \cdot \xi_w) = A \sin(\lambda \cdot \xi_w + \beta). \quad (\text{A1.26})$$

Condition (A1.26) is satisfied when

$$B = \frac{1}{\sin(\lambda \cdot \xi_w)} ; \quad A = \frac{1}{\sin(\lambda \cdot \xi_w + \beta)} .$$

β is obtained from the flux exchange at the interface given in Equations (A1.22) and (A1.17). It can be presented as

$$\beta_n = \cot^{-1}\left(\frac{(k_f - k_w)}{k_f \cdot \xi_w \cdot \lambda_n} + \frac{k_w \cot(\xi_w \cdot \lambda_n)}{k_f}\right) + i \cdot \pi - \xi_w \cdot \lambda_n. \quad (\text{A1.27})$$

where $i = 0, 1, 2, 3, \dots$

We restrict our analysis to the case when $i = 0$. The values of the eigenfunctions would be the same for other values of this parameter.

A countable set of positive eigenvalues λ_n is obtained from the solution to Equation (A1.21). This equation can be rearranged to:

$$\lambda \cos(\lambda + \beta) + h_0 \sin(\lambda + \beta) = 0. \quad (\text{A1.28})$$

Remembering (A1.25) we obtain the following expressions for v_n

$$v_n(\xi) = \begin{cases} \frac{\sin(\lambda_n \cdot \xi)}{\sin(\lambda_n \cdot \xi_w)} & \text{when } 0 \leq \xi \leq \xi_w \\ \frac{\sin(\lambda_n \cdot \xi + \beta_n)}{\sin(\lambda_n \cdot \xi_w + \beta_n)} & \text{when } \xi_w < \xi \leq 1. \end{cases} \quad (\text{A1.29})$$

Functions $v_n(R)$ are orthogonal with weight (see [28, 46] for details on orthogonality)

$$k = \begin{cases} k_w & \text{when } 0 \leq \xi \leq \xi_w \\ k_f & \text{when } \xi_w < \xi \leq 1. \end{cases} \quad (\text{A1.30})$$

This means that $\int_0^1 v_n(\xi) \cdot v_m(\xi) \cdot k \, d\xi = \delta_{nm} \cdot \|v_n\|^2$, where

$$\delta_{nm} = \begin{cases} 1 & \text{when } n = m \\ 0 & \text{when } n \neq m \end{cases}$$

The norm of v_n can be obtained from the expression

$$\begin{aligned} \|v_n\|^2 &= \int_0^1 v_n^2 \cdot k \cdot d\xi = \int_0^{\xi_w} \left(\frac{\sin(\lambda_n \cdot \xi)}{\sin(\lambda_n \cdot \xi_w)} \right)^2 k_w \, d\xi + \int_{\xi_w}^1 \left(\frac{\sin(\lambda_n \cdot \xi + \beta_n)}{\sin(\lambda_n \cdot \xi_w + \beta_n)} \right)^2 k_f \, d\xi \\ &= \frac{k_w}{2} \left(\xi_w \csc(\xi_w \cdot \lambda_n)^2 - \frac{\cot(\xi_w \cdot \lambda_n)}{\lambda_n} \right) \\ &\quad + \frac{k_f}{4} \csc(\beta_n + \xi_w \cdot \lambda_n)^2 \left(2 - 2\xi_w + \frac{-\sin(2(\beta_n + \lambda_n)) + \sin(2(\beta_n + \xi_w \cdot \lambda_n))}{\lambda_n} \right). \end{aligned} \quad (\text{A1.31})$$

Solution (A1.19) for $V(t, \xi)$ with $v_n(\xi)$ defined by (A1.29) satisfies the boundary conditions for (A1.15). The fact that functions $v_n(\xi)$ are orthogonal with the weight k makes it possible for us to expand functions in (A1.15) and initial conditions (A1.16) as:

$$f(\xi) = \frac{-\xi}{1 + h_0} = \sum_{n=1}^{\infty} f_n \cdot v_n(\xi) \quad (\text{A1.32})$$

$$F_0(\xi) = R_d \cdot \xi \cdot T_0(\xi \cdot R_d) = \sum_{n=1}^{\infty} q_n \cdot v_n(\xi) \quad (\text{A1.33})$$

$$R_d^3 \cdot \xi \cdot \tilde{P}(\xi) = \sum_{n=1}^{\infty} p_n \cdot v_n(\xi) \quad (\text{A1.34})$$

$$f_n = \frac{1}{\|v_n\|^2} \int_0^1 f(\xi) \cdot v_n(\xi) \cdot k \, d\xi = \frac{1}{\|v_n\|^2} \left(\int_0^{\xi_w} \frac{-\xi}{1 + h_0} \frac{\sin(\lambda_n \cdot \xi)}{\sin(\lambda_n \cdot \xi_w)} k_w \, d\xi + \int_{\xi_w}^1 \frac{-\xi}{1 + h_0} \frac{\sin(\lambda_n \cdot \xi + \beta_n)}{\sin(\lambda_n \cdot \xi_w + \beta_n)} k_f \, d\xi \right) \quad (\text{A1.35})$$

$$q_n = \frac{1}{\|v_n\|^2} \int_0^1 F_0(\xi) \cdot v_n(\xi) \cdot k \, d\xi = \frac{1}{\|v_n\|^2} \left(\int_0^{\xi_w} R_d \cdot \xi \cdot T_{w0}(\xi \cdot R_d) \frac{\sin(\lambda_n \cdot \xi)}{\sin(\lambda_n \cdot \xi_w)} k_w \, d\xi + \int_{\xi_w}^1 R_d \cdot \xi \cdot T_{f0}(\xi \cdot R_d) \frac{\sin(\lambda_n \cdot \xi + \beta_n)}{\sin(\lambda_n \cdot \xi_w + \beta_n)} k_f \, d\xi \right) \quad (\text{A1.36})$$

$$p_n = \frac{1}{\|v_n\|^2} \int_0^1 R_d^3 \cdot \xi \cdot \tilde{P}(\xi) \cdot v_n(\xi) \cdot k \, d\xi = \frac{1}{\|v_n\|^2} \left(\int_0^{\xi_w} R_d^3 \cdot \xi \cdot \tilde{P}(\xi) \frac{\sin(\lambda_n \cdot \xi)}{\sin(\lambda_n \cdot \xi_w)} k_w \, d\xi + \int_{\xi_w}^1 R_d^3 \cdot \xi \cdot \tilde{P}(\xi) \frac{\sin(\lambda_n \cdot \xi + \beta_n)}{\sin(\lambda_n \cdot \xi_w + \beta_n)} k_f \, d\xi \right) \quad (\text{A1.37})$$

Remembering (A1.15) and (A1.19), and using Equations (A1.32)-(A1.37) we can write

$$\sum_{n=1}^{\infty} (R_d^2(t) \cdot \theta'_n(t) + \kappa \cdot \lambda_n^2 \cdot \theta_n(t)) v_n(\xi) = \sum_{n=1}^{\infty} (f_n \cdot R_d^2(t) \cdot \mu'_0(t)) v_n(\xi) + \sum_{n=1}^{\infty} p_n \cdot v_n(\xi). \quad (\text{A1.38})$$

This equation is satisfied if and only if the coefficients on the two sides are equal, i.e.

$$R_d^2 \cdot \theta'_n(t) + \kappa \cdot \lambda_n^2 \cdot \theta_n(t) = f_n \cdot R_d^2 \cdot \mu'_0(t) + p_n. \quad (\text{A1.39})$$

(A1.39) needs to be solved using the initial condition

$$\theta_n(0) = q_n + f_n \cdot \mu_0(0). \quad (\text{A1.40})$$

The complementary solution to the homogeneous equation

$$R_d^2 \cdot \theta'_n(t) + \kappa \cdot \lambda_n^2 \cdot \theta_n(t) = 0,$$

using (A1.40), can be presented as:

$$\theta_n(t) = \theta_n(0) \exp\left(-\frac{\kappa \cdot \lambda_n^2 \cdot t}{R_d^2}\right).$$

Remembering (A1.40), this solution can be presented as:

$$\theta_n(t) = (q_n + \mu_0(0) \cdot f_n) \exp\left(-\frac{\kappa \cdot \lambda_n^2 \cdot t}{R_d^2}\right).$$

The particular solution to (A1.39) can be presented as

$$\theta_n(t) = (q_n + \mu_0(0) \cdot f_n) \exp\left(-\frac{\kappa \cdot \lambda_n^2 \cdot t}{R_d^2}\right) + \int_0^t \left(\frac{p_n}{R_d^2} + f_n \cdot \mu'_0(\tau)\right) \exp\left(\frac{\kappa \cdot \lambda_n^2 (\tau - t)}{R_d^2}\right) d\tau. \quad (\text{A1.41})$$

This allows us to obtain the final equation for temperature distribution inside the droplet:

$$T(\xi, t) = \frac{1}{R_d \cdot \xi} \sum_{n=1}^{\infty} \left(\theta_n(t) \cdot v_n(\xi) + \frac{\mu_0(t)}{1 + h_0} \xi \right). \quad (\text{A1.42})$$

This expression is the same as given in Formula (4.1).

Appendix B

The verification of the model using the prediction of the previously developed model for homogeneous droplets

To perform a comparison between the new model and the model described in [43], we assume that all properties of water are the same as those of fuel:

$$k_w = k_f; \quad \kappa_w = \kappa_f. \quad (\text{B1.1})$$

Using (A1.27), we obtain $\beta = 0$. The eigenfunctions $v_n(\xi)$, defined by (A1.29), become continuous functions and can be rewritten as

$$v_n(\xi) = \frac{\sin(\lambda_n \cdot \xi)}{\sin(\lambda_n \cdot \xi_w)} \quad \text{when } 0 \leq \xi \leq 1. \quad (\text{B1.2})$$

We introduce subscript (hom) to denote the functions for homogeneous droplets [30]:

$$v_n(\xi) = \frac{v_{n(\text{hom})}(\xi)}{\sin(\lambda_n \cdot \xi_w)}. \quad (\text{B1.3})$$

Using

(A1.31), $\|v_n\|^2$ can be rewritten as

$$\|v_n\|^2 = k_f \csc(\xi_w \cdot \lambda_n)^2 \frac{1}{2} \left(1 - \frac{\sin(2\lambda_n)}{\lambda_n} \right) \quad (\text{B1.4})$$

or

$$\|v_n\|^2 = k_f \csc(\xi_w \cdot \lambda_n)^2 \cdot \|v_n\|_{(\text{hom})}^2. \quad (\text{B1.5})$$

Using Equations (A1.35), (B1.3) and (B1.5), f_n can be rewritten as

$$f_n = \frac{1}{k_f \csc(\xi_w \cdot \lambda_n)^2 \cdot \|v_n\|_{(\text{hom})}^2} \int_0^1 \left(\frac{-\xi}{1+h_0} \right) \csc(\xi_w \cdot \lambda_n) v_{n(\text{hom})}(\xi) \cdot k_f d\xi.$$

This expression can be reduced to

$$f_n = \sin(\xi_w \cdot \lambda_n) \cdot f_{n(\text{hom})}. \quad (\text{B1.6})$$

Following the same procedure, we obtain the following expressions for q_n and $\theta_n(t)$:

$$q_n = \sin(\xi_w \cdot \lambda_n) \cdot q_{n(\text{hom})}, \quad (\text{B1.7})$$

$$p_n = \sin(\xi_w \cdot \lambda_n) \cdot p_{n(\text{hom})}, \quad (\text{B1.8})$$

$$\theta_n(t) = \sin(\xi_w \cdot \lambda_n) \cdot \theta_{n(\text{hom})}(t). \quad (\text{B1.9})$$

Recalling the definition of T_{eff} introduced in [43]

$$T_g + \frac{\rho_l \cdot L_f \cdot \dot{R}_d}{h} = T_{\text{eff}},$$

and using (A1.42), (B1.3) and (B1.9), the final equation for droplet heating reduces to

$$T(\xi, t) = \frac{1}{R_d \cdot \xi} \sum_{n=1}^{\infty} (\theta_n(t) \cdot v_n(\xi)) + T_{\text{eff}}. \quad (\text{B1.10})$$

This expression is the same as derived in [43] for heating and evaporation of a homogeneous droplet (see Equation (16) in this paper) if we do not take into account the contribution of radiative heating. This shows the consistency of our new model and the model developed in [43] for homogeneous droplets.

References

- [1] I. Glassman, R. A. Yetter, and N. G. Glumac, *Combustion*. Academic Press, 2015.
- [2] V. M. Ivanov and P. I. Nefedov, "Experimental Investigation of the combustion process of natural and emulsified liquid fuels," NASA TT F-258, 1965.
- [3] O. A. Elsanusi, M. M. Roy, and M. S. Sidhu, "Experimental Investigation on a Diesel Engine Fueled by Diesel-Biodiesel Blends and their Emulsions at Various Engine Operating Conditions," *Applied Energy*, vol. 203, pp. 582-593, 2017, doi: <https://doi.org/10.1016/j.apenergy.2017.06.052>.
- [4] A. M. A. Attia and A. R. Kulchitskiy, "Influence of the structure of water-in-fuel emulsion on diesel engine performance," *Fuel*, vol. 116, pp. 703-708, 2014, doi: <https://doi.org/10.1016/j.fuel.2013.08.057>.
- [5] P.-C. Chen, W.-C. Wang, W. L. Roberts, and T. Fang, "Spray and atomization of diesel fuel and its alternatives from a single-hole injector using a common rail fuel injection system," *Fuel*, vol. 103, pp. 850-861, 2013, doi: <https://doi.org/10.1016/j.fuel.2012.08.013>.
- [6] C. K. Law, *Combustion Physics*. Cambridge: Cambridge University Press, 2006.
- [7] C. K. Law, C. H. Lee, and N. Srinivasan, "Combustion characteristics of water-in-oil emulsion droplets," *Combustion and Flame*, vol. 37, pp. 125-143, 1980, doi: [https://doi.org/10.1016/0010-2180\(80\)90080-2](https://doi.org/10.1016/0010-2180(80)90080-2).
- [8] C. H. Wang, X. Q. Liu, and C. K. Law, "Combustion and microexplosion of freely falling multicomponent droplets," *Combustion and Flame*, vol. 56, no. 2, pp. 175-197, 1984, doi: [https://doi.org/10.1016/0010-2180\(84\)90036-1](https://doi.org/10.1016/0010-2180(84)90036-1).
- [9] A. Miglani, S. Basu, and R. Kumar, "Insight into instabilities in burning droplets," *Physics of Fluids*, vol. 26, no. 3, p. 032101, 2014, doi: <https://doi.org/10.1063/1.4866866>.
- [10] H. Watanabe and K. Okazaki, "Visualization of secondary atomization in emulsified-fuel spray flow by shadow imaging," *Proceedings of the Combustion Institute*, vol. 34, no. 1, pp. 1651-1658, 2013, doi: <https://doi.org/10.1016/j.proci.2012.07.005>.
- [11] J. C. Lasheras, A. C. Fernandez-Pello, and F. L. Dryer, "Experimental Observations on the Disruptive Combustion of Free Droplets of Multicomponent Fuels," *Combustion Science and Technology*, vol. 22, no. 5-6, pp. 195-209, 1980, doi: <https://doi.org/10.1080/00102208008952383>.
- [12] C. H. Wang and C. K. Law, "Microexplosion of fuel droplets under high pressure," *Combustion and Flame*, vol. 59, no. 1, pp. 53-62, 1985, doi: [https://doi.org/10.1016/0010-2180\(85\)90057-4](https://doi.org/10.1016/0010-2180(85)90057-4).
- [13] D. L. Zhu and C. K. Law, "Aerothermochemical studies of energetic liquid materials: 1. Combustion of HAN-based liquid gun propellants under atmospheric pressure," *Combustion and Flame*, vol. 70, no. 3, pp. 333-342, 1987, doi: [https://doi.org/10.1016/0010-2180\(87\)90112-x](https://doi.org/10.1016/0010-2180(87)90112-x).
- [14] T. X. Li, D. L. Zhu, and C. K. Law, "Droplet Combustion, Microexplosion, and Sooting Characteristics of Several Energetic Liquid Propellants," *Journal of Propulsion and Power*, vol. 14, no. 1, pp. 45-50, 1998, doi: <https://doi.org/10.2514/2.5264>.
- [15] D. V. Antonov, G. V. Kuznetsov, P. A. Strizhak, O. Rybdylova, and S. S. Sazhin, "Micro-explosion and autoignition of composite fuel / water droplets," *Combustion and Flame*, vol. 210, pp. 479-489, 2019, doi: <https://doi.org/10.1016/j.combustflame.2019.09.004>.
- [16] P. Cho, C. K. Law, and M. Mizomoto, "Effect of pressure on the micro-explosion of water/oil emulsion droplets over a hot plate," *Journal of Heat Transfer*, vol. 113, no. 1, pp. 272-274, 1991, doi: <https://doi.org/10.1115/1.2910545>.
- [17] H.-z. Sheng, L. Chen, and C.-k. Wu, "The Droplet Group Micro-Explosions in W/O Diesel Fuel Emulsion Sprays," *SAE International*, 1995, doi: <https://doi.org/10.4271/950855>.
- [18] J. C. Lasheras, L. T. Yap, and F. L. Dryer, "Effect of the ambient pressure on the explosive burning of emulsified and multicomponent fuel droplets," *Symposium (International) on Combustion*, vol. 20, no. 1, pp. 1761-1772, 1985, doi: [https://doi.org/10.1016/s0082-0784\(85\)80673-1](https://doi.org/10.1016/s0082-0784(85)80673-1).
- [19] T. Kadota and H. Yamasaki, "Recent advances in the combustion of water fuel emulsion," *Progress in Energy and Combustion Science*, vol. 28, no. 5, pp. 385-404, 2002, doi: [https://doi.org/10.1016/s0360-1285\(02\)00005-9](https://doi.org/10.1016/s0360-1285(02)00005-9).

- [20] E. Mura, P. Massoli, C. Josset, K. Loubar, and J. Bellettre, "Study of the micro-explosion temperature of water in oil emulsion droplets during the Leidenfrost effect," *Experimental Thermal and Fluid Science*, vol. 43, pp. 63-70, 2012, doi: <https://doi.org/10.1016/j.exptthermflusci.2012.03.027>.
- [21] Y. Suzuki, T. Harada, H. Watanabe, M. Shoji, Y. Matsushita, H. Aoki, and T. Miura, "Visualization of aggregation process of dispersed water droplets and the effect of aggregation on secondary atomization of emulsified fuel droplets," *Proceedings of the Combustion Institute*, vol. 33, no. 2, pp. 2063-2070, 2011, doi: <https://doi.org/10.1016/j.proci.2010.05.115>.
- [22] M. A. Ismael, M. R. Heikal, A. R. A. Aziz, M. El-Adawy, Z. Nissar, M. B. Baharom, E. Z. A. Zainal, Firmansyah, and C. Crua, "Investigation of puffing and micro-explosion of water-in-diesel emulsion spray using shadow imaging," *Energies*, vol. 11, no. 9, p. 2281, 2018, doi: <https://doi.org/10.3390/en11092281>.
- [23] J. Shinjo, J. Xia, L. C. Ganippa, and A. Megaritis, "Physics of puffing and microexplosion of emulsion fuel droplets," *Physics of Fluids*, vol. 26, no. 10, p. 103302, 2014, doi: <https://doi.org/10.1063/1.4897918>.
- [24] J. Shinjo, J. Xia, A. Megaritis, L. C. Ganippa, and R. F. Cracknell, "Modeling Temperature Distribution Inside an Emulsion Fuel Droplet Under Convective Heating: a Key To Predicting Microexplosion and Puffing," *Atomization and Sprays*, vol. 26, no. 6, pp. 551-583, 2016, doi: <https://doi.org/10.1615/AtomizSpr.2015013302>.
- [25] J. Shinjo, J. Xia, L. C. Ganippa, and A. Megaritis, "Puffing-enhanced fuel/air mixing of an evaporating n-decane/ethanol emulsion droplet and a droplet group under convective heating," *Journal of Fluid Mechanics*, vol. 793, pp. 444-476, 2016, doi: <https://doi.org/10.1017/jfm.2016.130>.
- [26] Y. Zhang, Y. Huang, R. Huang, S. Huang, Y. Ma, S. Xu, and Z. Wang, "A new puffing model for a droplet of butanol-hexadecane blends," *Applied Thermal Engineering*, vol. 133, pp. 633-644, 2018/03/25/ 2018, doi: <https://doi.org/10.1016/j.applthermaleng.2018.01.096>.
- [27] O. G. Girin, "Dynamics of the Emulsified Fuel Drop Microexplosion," *Atomization and Sprays*, vol. 27, no. 5, pp. 407-422, 2017, doi: <https://doi.org/10.1615/AtomizSpr.2017017143>.
- [28] S. S. Sazhin, O. Rybdylova, C. Crua, M. Heikal, M. A. Ismael, Z. Nissar, and A. R. B. A. Aziz, "A simple model for puffing/micro-explosions in water-fuel emulsion droplets," *International Journal of Heat and Mass Transfer*, vol. 131, pp. 815-821, 2019, doi: <https://doi.org/10.1016/j.ijheatmasstransfer.2018.11.065>.
- [29] S. Sazhin, *Droplets and Sprays*. London: Springer, 2014.
- [30] S. S. Sazhin, P. A. Krutitskii, I. G. Gusev, and M. R. Heikal, "Transient heating of an evaporating droplet," *International Journal of Heat and Mass Transfer*, vol. 53, no. 13, pp. 2826-2836, 2010, doi: <https://doi.org/10.1016/j.ijheatmasstransfer.2010.02.015>.
- [31] S. S. Sazhin, P. A. Krutitskii, I. G. Gusev, and M. R. Heikal, "Transient heating of an evaporating droplet with presumed time evolution of its radius," *International Journal of Heat and Mass Transfer*, vol. 54, no. 5, pp. 1278-1288, 2011, doi: <https://doi.org/10.1016/j.ijheatmasstransfer.2010.10.018>.
- [32] C. T. Avedisian and I. Glassman, "Superheating and boiling of water in hydrocarbons at high pressures," *International Journal of Heat and Mass Transfer*, vol. 24, no. 4, pp. 695-706, 1981, doi: [https://doi.org/10.1016/0017-9310\(81\)90013-2](https://doi.org/10.1016/0017-9310(81)90013-2).
- [33] C. T. Avedisian, "The Homogeneous Nucleation Limits of Liquids," *Journal of Physical and Chemical Reference Data*, vol. 14, no. 3, pp. 695-729, 1985, doi: <https://doi.org/10.1063/1.555734>.
- [34] T. Bar-Kohany and Y. Amsalem, "Nucleation Inception Temperature in Boiling due to Rapid Heating - A Universal Correlation," in *29th Conference on Liquid Atomization and Spray Systems*, Paris, France, ILASS-Europe, Ed., 2019.
- [35] X. Y. Liu, "Heterogeneous nucleation or homogeneous nucleation?," *Journal of Chemical Physics*, vol. 112, no. 22, pp. 9949-9955, 2000, doi: <https://doi.org/10.1063/1.481644>.
- [36] C. K. Law and G. M. Faeth, "Opportunities and challenges of combustion in microgravity," *Progress in Energy and Combustion Science*, vol. 20, no. 1, pp. 65-113, 1994, doi: [https://doi.org/10.1016/0360-1285\(94\)90006-x](https://doi.org/10.1016/0360-1285(94)90006-x).
- [37] H. D. E. Ross and S. R. R. Gollahalli, "Microgravity Combustion: Fire in Free Fall," *Applied Mechanics Reviews*, vol. 55, no. 6, pp. B116-B117, 2002, doi: <https://doi.org/10.1115/1.1508155>.
- [38] A. Faghri and Y. Zhang, *Transport Phenomena in Multiphase Systems*. Boston: Academic Press, 2006.
- [39] W. A. Sirignano, *Fluid Dynamics and Transport of Droplets and Sprays*. Cambridge: Cambridge University Press, 2010.
- [40] B. Abramzon and S. Sazhin, "Convective vaporization of a fuel droplet with thermal radiation absorption," *Fuel*, vol. 85, no. 1, pp. 32-46, 2006, doi: <https://doi.org/10.1016/j.fuel.2005.02.027>.

- [41] B. Abramzon and W. A. Sirignano, "Droplet vaporization model for spray combustion calculations," *International Journal of Heat and Mass Transfer*, vol. 32, no. 9, pp. 1605-1618, 1989, doi: [https://doi.org/10.1016/0017-9310\(89\)90043-4](https://doi.org/10.1016/0017-9310(89)90043-4).
- [42] R. B. Bird, W. E. Stewart, and E. N. Lightfoot, *Transport phenomena-2nd ed.* John Wiley & Sons, Ltd, 1961.
- [43] S. S. Sazhin, P. A. Krutitskii, W. A. Abdelghaffar, E. M. Sazhina, S. V. Mikhalovsky, S. T. Meikle, and M. R. Heikal, "Transient heating of diesel fuel droplets," *International Journal of Heat and Mass Transfer*, vol. 47, no. 14, pp. 3327-3340, 2004/07/01/ 2004, doi: <https://doi.org/10.1016/j.ijheatmasstransfer.2004.01.011>.
- [44] S. S. Sazhin, M. Al Qubeissi, and J. F. Xie, "Two approaches to modelling the heating of evaporating droplets," *International Communications in Heat and Mass Transfer*, vol. 57, pp. 353-356, 2014, doi: <https://doi.org/10.1016/j.icheatmasstransfer.2014.08.004>.
- [45] D. V. Antonov, O. V. Vysokomornaya, M. V. Piskunov, R. M. Fedorenko, and W. M. Yan, "Influence of solid nontransparent inclusion shape on the breakup time of heterogeneous water drops," *International Communications in Heat and Mass Transfer*, vol. 101, pp. 21-25, 2019, doi: <https://doi.org/10.1016/j.icheatmasstransfer.2018.12.009>.
- [46] S. S. Sazhin, I. G. Gusev, P. A. Krutitskii, and M. R. Heikal, "Transient heating of a semitransparent spherical body immersed into a gas with inhomogeneous temperature distribution," *International Journal of Thermal Sciences*, vol. 50, no. 7, pp. 1215-1222, 2011, doi: <https://doi.org/10.1016/j.ijthermalsci.2011.02.012>.